RUHUNA JOURNAL OF SCIENCE
Vol 13 (2): 92-109, December 2022
eISSN: 2536-8400
http://doi.org/10.4038/rjs.v13i2.118

Faculty of Science
University of Ruhuna
SRI LANKA

Qualitative mineralogical analysis of Barracuda exploration well in the offshore Mannar Basin (the Indian Ocean) using FTIR and XRD techniques

B.M. Gunathilake [1], D.T. Jayawardana [2], A.S. Ratnayake [3] and A.M.N.M. Adikaram [4]

[1,2] *Department of Forestry and Environmental Science, Faculty of Applied Sciences, University of Sri Jayewardenepura, Sri Lanka*
[3] *Department of Applied Earth Sciences, Faculty of Applied Sciences, Uva Wellassa University, Sri Lanka*
[4] *Department of Physical Sciences, Faculty of Applied Science, South-Eastern University, Sri Lanka*

*Correspondence: [1]bhanukagunathilake@sjp.ac.lk; ORCID https://orcid.org/0000-0002-1204-4954

Received: 15th December 2021, Revised: 28th September 2022, Accepted: 3rd November 2022

Abstract The Mannar Basin plays a vital role in petroleum exploration in Sri Lanka, and its Barracuda exploration well was drilled up to 4206 m in depth. The objective of the current study is to identify mineralogy using Fourier-transform infrared (FTIR) and X-ray diffraction (XRD) analyses. The FTIR and XRD analyses confirm the presence of quartz, feldspar, clay minerals (e.g., kaolinite, montmorillonite), calcite, and hematite in all marlstone and mudstone samples. These sedimentary rocks can be identified as potential petroleum source rocks in the Mannar Basin. Quartz, carbonate, and hematite cementations are directly reduced porosity and permeability, and thus primary migration of hydrocarbons from potential source rocks. Clay minerals act as a seal for hydrocarbon migrations in the Mannar Basin. A variety of dominant clay mineral assemblages allows the reconstruction of several paleoclimatic chronozones in warm/wet and arid climates. In contrast, feldspar dissolution promotes the primary migration of hydrocarbon from potential petroleum source rocks. Consequently, this study concluded that common minerals such as quartz, carbonate, and hematite are associated with the trapping and binding processes of hydrocarbons.

Keywords: Cementation, clay mineral, petroleum source rock, primary hydrocarbon migration

1 Introduction

The Mannar Basin is the main sedimentary archive for petroleum exploration in Sri Lanka (Kularathna *et al*. 2020). It is a prolific producer of both gas and oil in the currently explored deep-water area. This basin contains a thick succession of sediments from the Upper Jurassic to the recent age (Ratnayake, 2021a). The regional tectonic settings have significantly impacted the distribution of sedimentary strata (Ratnayake *et al*. 2014). Source rock quality, maturity, and reservoir rocks play vital roles in evaluating oil and gas potential (Jiang *et al*. 2015, Ratnayake *et al*. 2018, Ratnayake, 2022), and mineralogy is a crucial part of understanding the primary migration of hydrocarbon from the source rocks. For example, the source rock fragility and cementation are affected by minerals such as quartz, feldspar, and carbonate (Zou *et al*. 2010, Liang *et al*. 2014).

Quartz is one of the most abundant minerals in the earth's crust, and it plays an essential role in sediment composition and diagenesis. As a result, quartz is frequently used in mineralogical studies to determine provenance (Bahlburg and Floyd 1999, Bernet and Basset 2005). The differential brittleness and dissolution nature of feldspar also influence the porosity and permeability of the petroleum source rocks (Xu *et al*. 2013). The porosity and permeability of the hydrocarbon source rocks have a good relationship with the feldspar minerals due to mechanical characteristics such as brittleness and degree of cleavage development (Xu *et al*. 2013). The diagenetic variations in clay minerals and composition are used to examine primary migration and the thermal history of sedimentary basins (Pollastro and Bohor 1993, Xu *et al*. 2013). Clay minerals are also used in paleoclimatic studies (Dera *et al*. 2009, Leontopoulou *et al*. 2019). In addition, clay minerals act as a catalyst and adsorbents in petroleum production (Xu *et al*. 2013). Furthermore, carbonate minerals play an essential role in predicting hydrocarbon receiver quality, such as the permeability and porosity of petroleum source rocks (Chen *et al*. 2019).

The Mannar Basin, which stretches from southeast India to southwest-northeast Sri Lanka, has a total area of 45,000 km^2 (Figure 1). The basement of the basin is made up of Precambrian high-grade metamorphic rocks (Cooray 1984, Ratnayake *et al*. 2014, Kularathna *et al*. 2020). The tectonostratigraphic evolution of the Mannar Basin can be split into three phases: pre-rift, rift, and post-rift (Ratnayake 2021b). The middle Jurassic to Early Cretaceous period is known as the early and late rift phases. In addition, the early rifting of the Mannar Basin was linked to the late stratification of eastern and western Gondwana during the middle Jurassic (Ratnayake and Sampei 2015, Kularathna *et al*. 2020). The rift phase was linked with the thermal sag during the Late Cretaceous, and the post-rift phase was identified in the Oligocene and Miocene (Kularathna *et al*. 2020). From the Jurassic to the present, multiple rifting processes caused to deposit of terrestrial and marine sediments in the offshore Manner Basin over 167 million years.

The horsts, skewed fault blocks, and compression-induced traps originated mainly during the rifting process, and they offer significant exploration potential in this basin (Ratnayake *et al*. 2018). The current covering of sediment around the Mannar Basin reaches 6 km in thickness (Kularathna *et al*. 2020). Major rifting events occurred during the Late Cretaceous due to the separation of Madagascar, Laxmi

Ridge/Seychelles, and Seychelles from the Indian Plate (Chatterjee *et al*. 2013). Both intrusive and extrusive igneous origins were influenced by this sequential separation (Ratnayake *et al*. 2014, Kularathna *et al*. 2020). Furthermore, carbonate-rich sediments from the Late Paleocene were discovered in the Mannar Basin, showing that the continental climate shifted from temperate to tropical as it traveled to the northward equator. Moreover, several studies have suggested the Mannar Basin is a sub-basin of the Cauvery Basin due to similarities in tectonic settings, geology and stratigraphy (Rao *et al*. 2010).

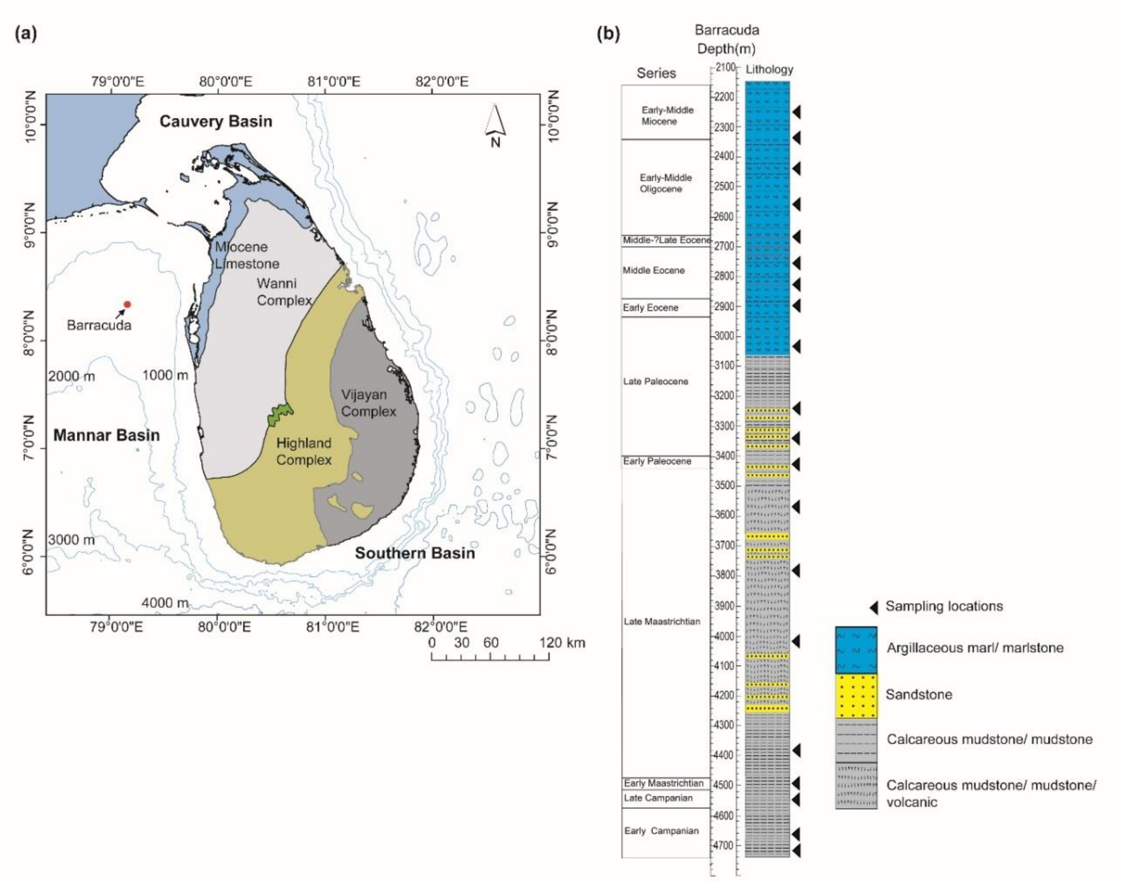

Fig 1. a) Simplified geological map of Sri Lanka showing the locations of hydrocarbon exploration wells in the Mannar Basin, and b) lithostratigraphic successions of Barracuda exploration well with sampling locations (modified after Ratnayake *et al*. 2018)

In the deep-water Mannar Basin, Cairn Lanka Private Limited conducted drilling activities in exploration block SL 2007-01-001 (Ratnayake *et al*. 2017). Cairn drilled three exploration wells (Dorado, Dorado North, and Barracuda) in 2011 and one exploration well (Wallago) in 2013 (Figure 1). Due to a technical issue, the Wallago exploration well was eventually abandoned before reaching the desired drilling depth (Ratnayake *et al*. 2017). The first natural gas finding in Sri Lanka was made in Campanian sandstones of the Dorado well at depths of 3044–3069 m (total thickness of 25 m). The second discovery was made in the Upper Cretaceous sandstones of the Barracuda well at depths of 4,067–4,206 m (total thickness = 24 m) (Ratnayake *et al*. 2017, Kularathna *et al*. 2020). However, mineralogical characteristics in the Mannar Basin are not investigated yet. Consequently, the primary objective of this research is to conduct a qualitative mineralogical examination of potential petroleum source rocks in the Barracuda exploration well in the offshore Mannar Basin (the Indian Ocean).

2 Materials and Methods

2.1 Sample collection and preparation

Sediment samples were collected from the Barracuda well (sampling depth of 2139–4741 m) during the hydrocarbon exploration project in the Mannar Basin, conducted by the Petroleum Resources Development Secretariat (PRDS) Sri Lanka (Figure 1). The present study considered 20 representative calcareous argillaceous to arenaceous sediments from Late Cretaceous to Miocene. Samples were cleaned manually using 250 ml dichloromethane: methanol 9:1 v/v solution (Ratnayake and Sampei 2019). The cleaning efficiency was improved by washing samples twice with 50 ml aliquots of dichloromethane: methanol 9:1 solution. Twenty samples were cleaned and dried in a fume closet for 24 hours at room temperature. After that, cleaned samples were powdered using a motor and petal and sieved through a 53 µm standard sieve.

2.2 Sample analysis

Fourier-Transform Infrared (FTIR) analysis

A Bruker Vertex 80 FT-IR Spectrometer with an attenuated total reflection (ATR) sampling module and a diamond crystal plate at Sri Lanka Institute of Nanotechnology were used for FTIR measurements. Data were collected using the Opus software program, which was also utilized to adjust the background and baseline of each spectrum. Samples were scanned between 4000 and 400 cm^{-1} with a resolution of 4 cm^{-1}, and spectra were converted to absorbance mode. Three repetitions were carried out to ensure that spectra collected on selected samples had similar peak positions and absorbance intensities. The raw FTIR data were interpreted by determining peak positions using the literature.

X-Ray Diffraction (XRD) analysis

The selected samples were analyzed through a Rigaku Ultima IV X-ray diffractometer with Cu Kα radiation (λ = 1.54056) at Uva Wellassa University. The diffractograms were recorded at a scanning rate of 0.02°/second in the range of 0° to 80° 2θ. The observed XRD peaks were identified with International Centre for Diffraction Data (ICDD), Inorganic Crystal Structure Database (ICSD), and Crystallography Open Database (COD) using Crystal Impact Match 3.0 software and available literature.

3 Results

3.1 FTIR interpretations

FTIR spectra provide a qualitative examination of materials based on band types and positions of functional groups. The positions of observed absorption bands in each sample with wavenumber (cm^{-1}), their lithology, and age are shown in Table 1. The Barracuda well sediments contain characteristic peaks for silicates, carbonates, and O-H stretching. Different lithologies, including marlstone, marlstone with black carbon, calcareous mudstone, and argillaceous marlstone, are observed in the Barracuda well (Figure 2).

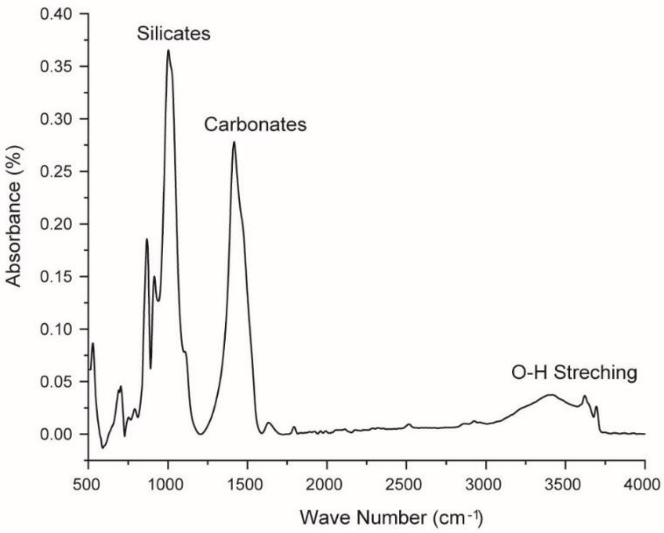

Fig 2. Typical FTIR spectrum of the Mannar Basin sediments (sample no. BRC 1 sample, depth from 2260–2270 m)

All these lithologies exhibit characteristic peaks for silicates, calcite, feldspar, montmorillonite, and kaolinite (Figure 3). Silicates are characterized by Si-O stretching and bending vibrations between 800–1200 cm^{-1} and 400–600 cm^{-1} (Sivakumar *et al*. 2012). The vibrational modes of carbonates (CO_3^{2-} ions) have an absorption band between 1400–1500 cm^{-1}. The peak at 798–780 cm^{-1} is due to Si-O-Si inter tetrahedral bridging bonds in quartz and O-H stretching vibrations at 3400–3750 cm^{-1} (Sivakumar *et al*. 2012, Xu *et al*. 2013). The weak absorption band at 1000–1800 cm^{-1} and 2500–3000 cm^{-1} are due to C=O, C-O, and aliphatic carbon (C-H) functional groups, respectively (Painter *et al*. 1981, Sivakumar *et al*. 2012). The summary of FTIR band assignments for identified different minerals in Barracuda well sediments is shown in Table 2.

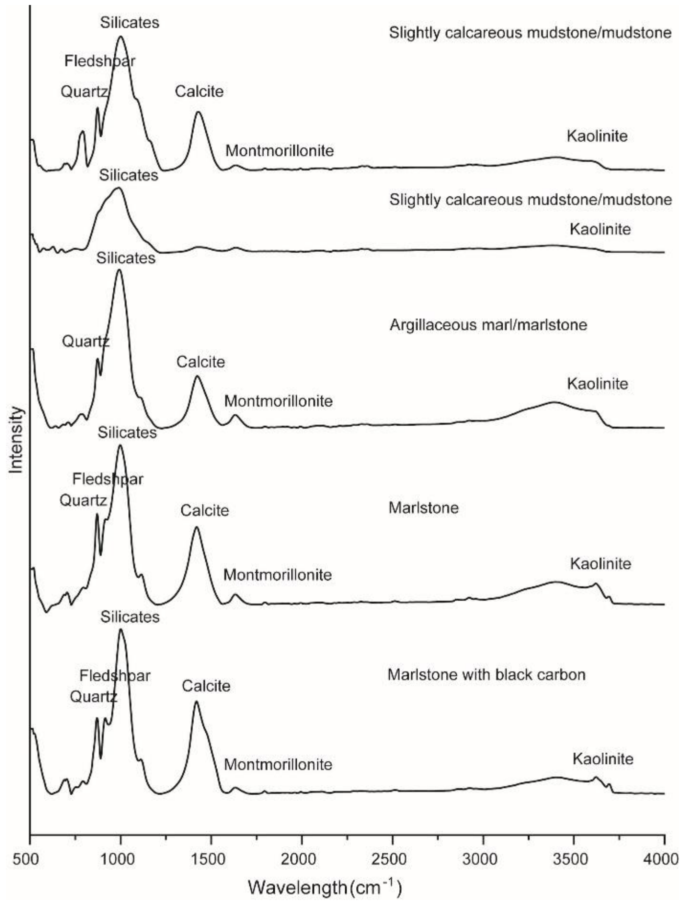

Fig 3. Representative FTIR spectra based on the lithology of Mannar Basin, Sri Lanka

Table 1: FTIR observations with the sample depth, age, and lithology of Barracuda well sediments.

Sample Number	Sample Depth (m)	Lithology	Age	Silicate Minerals	Feldspar		Clay Minerals		Carbonate Minerals
				Quartz	*Microcline*	*Orthoclase*	*Kaolinite*	*Montmorillonite*	*Calcite*
BRC 1	2260–2270	Marlstone with black carbon	Early Middle Miocene	460, 694, 793	460	–	914, 1006, 1002, 3621, 3694	3405	873, 1420, 1633, 1794, 2514
BRC 2	2350–2360	Marlstone with black carbon	Early Middle Miocene	692, 792	462	439	916, 1002, 3624, 3694	3405	871, 1418, 1632, 1795, 2514
BRC 3	2440–2450	Marlstone with black carbon	Early Middle Miocene	460, 792	460, 538, 1113	438, 538	914, 1113, 3622, 3694	3406	872, 1419, 1794, 2513
BRC 4	2560–2570	Marlstone	Early Middle Miocene	462,790	462		914, 1000, 3621, 3691	3407	871, 1416, 1632, 1795, 2512
BRC 5	2670–2680	Marlstone	Middle-Late Eocene	692, 793	–	539	913, 1004, 1109, 3620, 3693	3407	872, 1423, 1634, 1795, 2514
BRC 6	2760–2770	Marlstone	Middle Eocene	465, 684	–	–	3624, 3698	3403	871, 1420, 1632, 2512
BRC 7	2830–2840	Argillaceous marl/ marlstone	Middle Eocene	462, 682	–	–	914, 1002, 3624, 3690	3407	873, 1424, 1634, 2513
BRC 8	2900–2910	Argillaceous marl/ marlstone	Early Eocene	460, 685	–	–	912, 1000, 3619, 3689	3401	873, 1424, 2514
BRC 9	3030–3040	Argillaceous marl/ marlstone	Late Paleocene	467, 690	638	539	914, 1002, 3620, 3692	3402	874, 1422, 1632, 2514

Table 1. Continued

Sample Number	Sample Depth (m)	Lithology	Age	Silicate Minerals	Feldspar		Clay Minerals		Carbonate Minerals
				Quartz	*Microcline*	*Orthoclase*	*Kaolinite*	*Montmorillonite*	*Calcite*
BRC 10	3240–3250	Slightly calcareous mudstone/ mudstone	Late Paleocene	691	–	541	914, 1001 3620, 3694	3391,	874, 1426
BRC 11	3320–3330	Slightly calcareous mudstone/ mudstone	Late Paleocene	685, 786	1113	–	1113, 3624	3403	873, 1416, 1632
BRC 12	3420–3430	Slightly calcareous mudstone/ mudstone	Early Paleocene	463	–	434, 588	1000	3405	875, 1422, 1632, 2514
BRC 13	3570–3580	Slightly calcareous mudstone/ mudstone	Late Maastrichtian	465	–	547	–	3405	1424, 1634
BRC 14	3790–3800	Slightly calcareous mudstone/ mudstone	Late Maastrichtian	463	–	542, 581	1000	3410	875, 1422
BRC 15	4020–4030	Slightly calcareous mudstone/ mudstone/ volcanic	Late Maastrichtian	–	–	541,583	–	3404	1636
BRC 16	4380–4390	Slightly calcareous mudstone/ mudstone	Late Maastrichtian	694, 779–797	–	439, 538	1007	3402	873, 1425, 1634, 2512
BRC 17	4490–4500	Slightly calcareous mudstone/ mudstone	Early Maastrichtian	691,792	–	–	1014, 3615, 3698	3407	864, 1400, 1636, 1795, 2512
BRC 18	4540–4550	Slightly calcareous mudstone/ mudstone	Early Campanian	461, 792	–	–	3698	3403	871, 1410, 1636, 1793, 2512
BRC 19	4670–4680	Slightly calcareous mudstone/ mudstone	Early Campanian	693, 778–797		439, 546	1006	3400	873, 1426, 1636, 1795
BRC 20	4730–4740	Slightly calcareous mudstone/ mudstone	Early Campanian	693, 788	–	–	–	3401	873, 1422, 1632, 1797, 2512

Table 2: FTIR band assignments for identified different minerals in Barracuda well sediments.

Minerals	Wave number (cm^{-1})	Tentative assignments	References
Quartz	460, 694, 793, 685, 786, 788, 778, 797	Si-O symmetric bending, Si-O symmetric stretching	Kumar and Rajkumar (2020), Russell and Fraser (1987), Chester, R. and Elderfield, H., (1968)
Feldspar	421, 434, 460, 538, 541, 588, 638, 1113	Al-O coordination, Si-O stretching, O-H bending, O-H stretching, O-H	Ghosh (1978), Kumar and Rajkumar (2020), Russell and Fraser (1987)
Kaolinite	915, 3624, 3695	Si-O deformation, O-H deformation, O-H stretching	Russell and Fraser (1987), Hlavay *et al*., (1978), Kumar and Rajkumar (2020)
Montmorillonite	3405	O-H Stretching of absorbed water molecule	Russell and Fraser (1987)
Calcite	875, 1422, 1636, 2514	C=O stretching mode vibration, doubly degenerate asymmetric stretching, O-H stretching mode vibration, mode vibration	Chester, R. and Elderfield, H., 1968, Farmer (1974), Kumar and Rajkumar (2020)

3.2 XRD interpretations

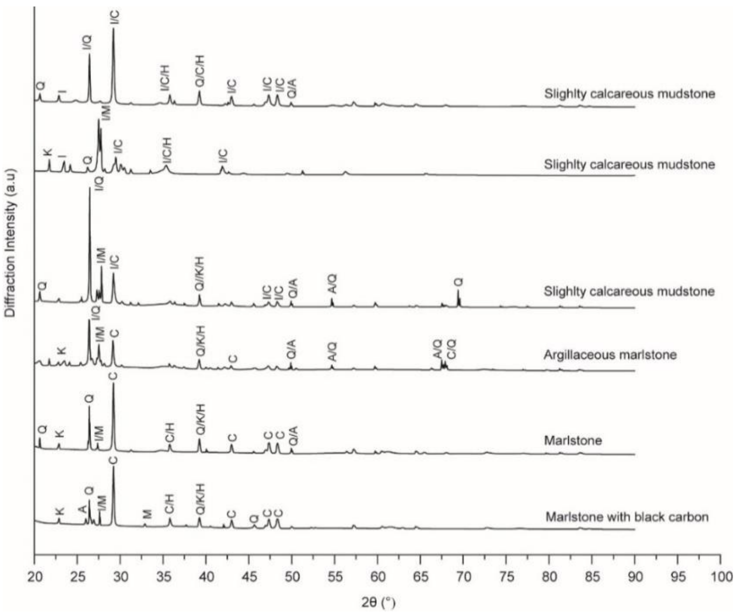

Fig 4. Representative XRD diffractograms based on the lithology of Mannar Basin
(Q: quartz, K: kaolinite, M: montmorillonite, C: calcite, I: illite, H: hematite, A: albite)

XRD analysis revealed the presence of quartz, albite, calcite, kaolinite, montmorillonite, illite, and hematite (Table 3 and Figure 4). XRD spectra show that calcite and quartz are dominant in marlstone. Quartz, illite, and calcite are dominant in argillaceous marlstone (Table 3). Illite, montmorillonite, kaolinite, and calcite dominate slightly in calcareous mudstone (Figure 4) (e.g. Butt 2012, Vaniman *et al*. 2014, Rampe *et al*. 2017).

Table 3: XRD peak positions (2θ values) and corresponding mineral phases in Barracuda well sediments

Sample Number	Sample Depth (m)	Lithology	Age	XRD (2Θ) Value						
				Quartz	Albite	Kaolinite	Montmorillonite	Illite	Calcite	Hematite
BRC 1	2260 – 2270	Marlstone with black carbon	Early Middle Miocene	26.4, 39.2, 45.6	26.0	22.8, 27.0, 39.2	27.0, 32.8	27.5	22.8, 29.2, 35.8, 42.9, 47.3, 48.2, 56.2, 57.3	35.8
BRC 2	2350 –2360	Marlstone with black carbon	Early Middle Miocene	26.4, 39.2, 45.6	26.0, 32.8	22.8, 42.0	27.6	27.5	29.2, 35.8, 43.0, 47.3, 48.4	35.8
BRC 4	2560 –2570	Marlstone	Early Middle Miocene	26.4, 39.2	–	22.8, 39.2	27.5	27.5	29.2, 35.8, 42.9, 48.3	35.8, 39.2
BRC 5	2670 –2680	Marlstone	Middle-Late Eocene	26.4, 39.2	–	22.8, 39.2	27.8	27.8	29.2, 35.7, 43.0, 47.3, 48.3	35.7
BRC 6	2760 –2770	Marlstone	Middle Eocene	20.6, 26.4, 39.2		22.8, 39.2	27.3	27.3	29.2, 35.7, 42.9, 47.3, 48.3	35.7
BRC 7	2830 –2840	Argillaceous marl/ marlstone	Middle Eocene	20.6, 26.4, 39.2, 49.9, 59.7	–	–	–	–	29.2, 36.2	–
BRC 8	2900 –2910	Argillaceous marl/ marlstone	Early Eocene	26.4		40.1	27.8	27.8	29.2, 35.7, 41.9	–

Table 3. Continued

Sample Number	Sample Depth (m)	Lithology	Age	XRD (2Θ) Value						
				Quartz	Albite	Kaolinite	Montmorillonite	Illite	Calcite	Hematite
BRC 9	3030 –3040	Argillaceous marl/ marlstone	Late Paleocene	26.4, 49.8	–	22.9	–	–	29.2, 35.8, 43.0, 47.4, 48.3	–
BRC 11	3320 –3330	Slightly calcareous mudstone/ mudstone	Late Paleocene	21.7, 26.3, 49.2, 54.6, 59.7, 67.5	–	39.2	27.5	–	29.1, 35.7	–
BRC 12	3420 –3430	Slightly calcareous mudstone/ mudstone	Early Paleocene	20.6, 26.4, 49.9, 54.6, 69.4	–	39.2	27.8	27.8	29.2	–
BRC 13	3570 –3580	Slightly calcareous mudstone/ mudstone	Late Maastrichtian	21.7, 26.4, 56.3	30.1	21.7, 24.2, 41.9	5.6, 27.5	23.4, 33.5	29.5	–
BRC 15	4020 –4030	Slightly calcareous mudstone/ mudstone/ volcanic	Late Maastrichtian	26.2	30.1, 51.3	21.7, 24.1, 35.3, 41.9	5.6, 27.5	23.4, 33.5	29.4	–
BRC 17	4490 –4500	Slightly calcareous mudstone/ mudstone	Early Maastrichtian	26.4	–	20.6, 22.8, 39.2	–	29.2, 35.8, 43.0, 47.3, 48.3	29.2, 35.8, 43.0, 47.3, 48.3	–
BRC 18	4540 –4550	Slightly calcareous mudstone/ mudstone	Early Campanian	20.6	–	12.1, 20.6, 22.8, 26.4, 39.2	–	26.4, 29.2, 35.8, 43.0, 47.3, 48.3	29.2, 35.8, 43.0, 47.3, 48.3	–
BRC 20	4730 –4740	Slightly calcareous mudstone/ mudstone	Early Campanian	20.6, 26.4	–	20.6, 26.4, 39.2	–	26.4, 29.1, 48.2	29.1	–

4 Discussion

4.1 The impact of the presence of quartz

FTIR spectra reveal an extreme absorption band in the 900–1100 cm^{-1} wavelength range due to Si-O strong bonds in the quartz silicate structure and less intense bands in the 400–800 cm^{-1} wavelength range. These brands such as 463 cm^{-1}, 694 cm^{-1}, 778 cm^{-1}, 793 cm^{-1}, 797 cm^{-1} and a doublet peak at 779–797 cm^{-1} were probably related to quartz (Sivakumar *et al*. 2012, Kumar and Rajkumar 2014). The distinct doublet peak, also known as the characteristic of quartz, can be observed in 4380–4390 m depth sample. Symmetrical bending and symmetrical stretching vibrations of Si-O can be identified at 695 cm^{-1} and 800 cm^{-1}, respectively (Hlavay *et al*. 1978, Sivakumar *et al*. 2012).

In this study, detrital quartz grains are subangular to subround and poorly to moderately sorted in an authigenic matrix. The typical authigenic cement of the Baracuda well is around 10%. Quartz is a generally detrital and authigenic mineral (Milliken 2014, Dowey and Taylor 2017). Quartz cement can be formed from the dissolution of biogenic amorphous silica, volcanic rock fragments, alteration of clay minerals, and dissolved feldspar grains. These processes are governed by internal and external resources (McBridge 1989, Worden and Morad 2000). Several studies show that quartz mineral affects the hydrocarbon reservoir and source rock quality (Worden and Morad 2000). The compaction of mudstones is influenced by quartz cementation (White *et al*. 2011, Peng *et al*. 2020). Quartz cementation is thus a significant process to reduce porosity and permeability (Worden and Morad 2000, Dowey and Taylor 2017). Therefore, quartz cementation has an impact on the primary mitigation of hydrocarbon in mudstones of the Mannar Basin.

4.2 The impact of the presence of feldspar

The bands observed at 421 cm^{-1}, 434 cm^{-1}, 438 cm^{-1}, 439 cm^{-1}, 460 cm^{-1}, 538 cm^{-1}, 539 cm^{-1}, 541 cm^{-1}, 546 cm^{-1}, 581 cm^{-1}, 583 cm^{-1}, 588 cm^{-1}, 638 cm^{-1} can probably indicate the presence of feldspar (Sivakumar *et al*. 2012, Kumar and Rajkumar 2014). The Si-O stretching mode vibrations cause an absorbance band at 640–645 cm^{-1} (Sivakumar *et al*. 2012). The Al-O vibration causes the orthoclase absorbance band at 635 cm^{-1}. The frequency at around ~440 cm^{-1} is due to O-H bending vibration (Sivakumar *et al*. 2012, Kumar and Rajkumar 2014). In this study, major types of felspar such as microcline, orthoclase, and albite can be predicted according to the band wavelength. However, albite was infrequent, while orthoclase and microcline forms predominated in several marlstone and mudstone samples (Table 1).

The Barracuda well sediments contain a variety of feldspar group minerals such as microcline and orthoclase. Feldspar alteration affects the evolution of permeability and porosity in sedimentary rocks (Kampman *et al*. 2009, Ruiz-Agudo *et al*. 2016). Therefore, feldspar dissolution can increase secondary porosity (Yuan *et al*. 2019). Accordingly, the secondary porosity increases the possible primary and secondary migration of oil and gas hydrocarbon. The degree of brittleness and dissolution of feldspar differs due to variations in crystal structure and chemical composition (Xu *et al*. 2013). However, feldspar alteration affects a significant impact on the permeability and porosity of source rocks and tight oil reservoirs.

4.3 The impact of the presence of clay minerals

The presence of kaolinite indicates the band detected at 915 cm^{-1}, 3623 cm^{-1}, and 3695 cm^{-1} due to the O-H stretching of the inner hydroxyl group (Sivakumar *et al*. 2012, Kumar and Rajkumar 2014). The amount of kaolinite varies with lithology. Therefore, the band intensity also changes from sample to sample (Kumar and Rajkumar 2014). The FTIR absorption peaks at 3405 cm^{-1} indicate the presence of montmorillonite clay (Russell and Fraser 1994, Sivakumar *et al*. 2012). This is due to water molecules vibrating in the O-H stretching mode. The intense FTIR peaks for montmorillonite and kaolinite were identified in all marlstone and mudstone samples. Therefore, montmorillonite, illite, and kaolinite are dominant clay minerals in Barracuda well sedimentary rocks in the Mannar Basin.

Montmorillonite, illite, and kaolinite are dominant clay minerals in sedimentary rocks of the Mannar Basin. The average clay percentage is ca. 20% in the Barracuda exploration well. Clay minerals in sedimentary basins are detrital or authigenic in origin (Raigemborn *et al*. 2014, Kumari and Mohan 2021). Clay minerals promote organic matter preservation in sedimentary rocks (Hossain *et al*. 2022). Additionally, the presence of expanding clays has specific catalytic effects on the production of oil as shown in oil shales. These clay minerals are also important in predicting tectonics, basin evolution history, and paleoclimate.

According to the predominant clay mineral assemblages, several paleoclimatic chronozones can be predicted in the Mannar Basin (Fig. 5). Montmorillonite-dominant strata from the Early Campanian indicate an arid climate. Kaolinite-dominant strata from the Late Campanian to Late Maastrichtian strata indicate warm and wet paleoclimate (Fig. 5). However, short-term global cooling events can also be predicted during the Late Maastrichtian. It shows that Early-Late Paleocene sediments from the Barracuda well indicate an arid climate in the Indian Ocean. The Early Eocene to Middle-Late Eocene age sediments is characterized by kaolinite-dominant clay. Therefore, it suggests the warm and wet greenhouse paleoclimate in the Indian Ocean. Kaolinite-dominant Early to middle Miocene sediments can suggest wet climatic conditions.

Hydrocarbon migration and accumulation are also controlled by clay minerals. For example, clay minerals provide an effective seal for the reservoir rocks (Zeng and Yu 2006, Jiang *et al*. 2015). In addition, clay minerals accelerate porosity reduction in both sandstone and limestone reservoir rocks in the Mannar Basin.

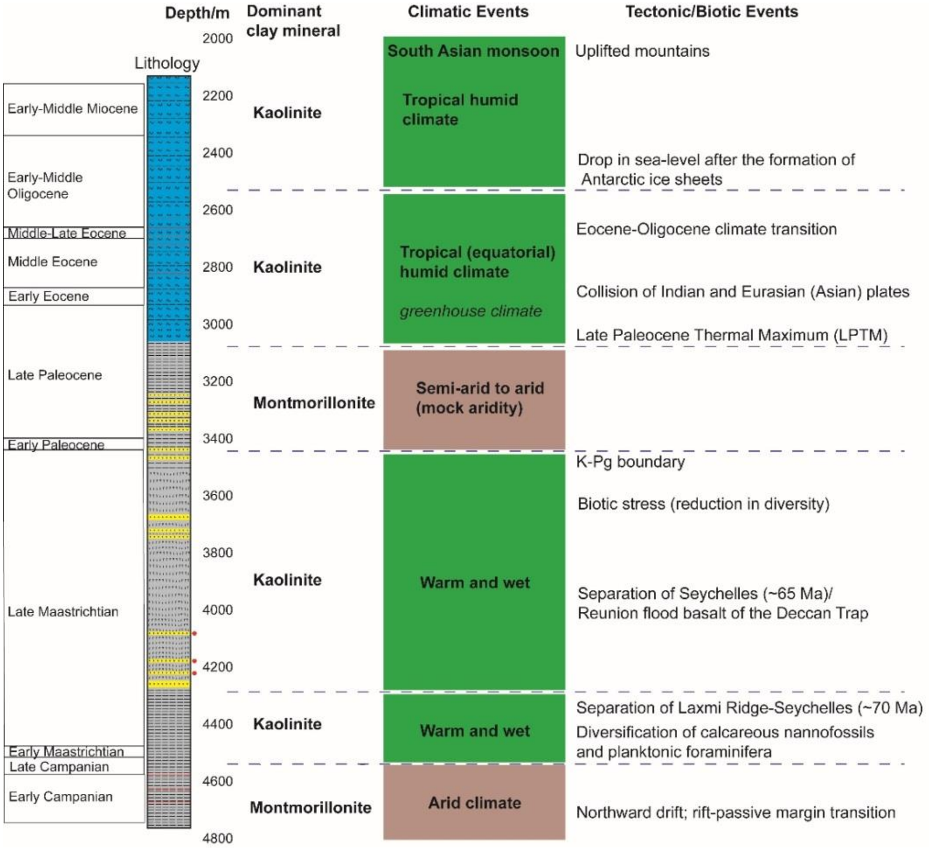

Fig 5. Relationship between clay mineralogy and recorded regional tectonic/biotic/climatic events

4.4 The impact of the presence of carbonate minerals

The absorbance bands appearing at 876 cm^{-1}, 1422 cm^{-1}, 1792 cm^{-1} and 2516 cm^{-1} are probably linked to calcite wavelengths (Sivakumar *et al*. 2012, Kumara and Rajkumar 2014), because of the stretching vibration of C=O has the IR band between 876 and 1792 cm^{-1}. The O-H stretching mode vibrations cause the band at 1422 cm^{-1}, and the doubly degenerate asymmetric stretching mode vibrations cause the band at 2516 cm^{-1} (Sivakumar *et al*. 2012, Kumar and Rajkumar 2014).

Calcite is the predominant carbonate mineral in all studied samples (Fig. 4). In addition, calcite is a distinguish mineral to identify main lithological changes (i.e., from between calcareous mudstones/mudstones/interbedded sandstone in the lower sedimentary succession to argillaceous marl/marlstone in the upper sedimentary succession) of the Barracuda exploration well (Ratnayake *et al*. 2014). Calcite can be formed by various mechanisms such as an authigenic mineral and weathered carbonate rock fragments (Pszonka and Wendorff 2017, Chen *et al*. 2019). Furthermore, microorganisms like coccolithophores and foraminifera play a significant role in the formation of calcite-dominant sediments (e.g., Zachos *et al*. 2001). The presence of sedimentary carbonate rocks can indicate the revisor quality strata for hydrocarbon accumulation in the Mannar Basin. However, carbonate cementation reduces the primary migration of hydrocarbons in the source rocks of the Mannar Basin.

4.5 The impact of the presence of hematite

Hematite is found in sedimentary rocks as detrital particles or chemical precipitates (Cornell and Schwertmann 2003). Quartz, feldspar, carbonate, and clay mineral cementation processes are common in sedimentary basins, whereas hematite cementation is uncommon (Chima *et al*. 2018). The hematite cement precipitates immediately in the interfacial pore space or line on grain surfaces. Previous research suggests that a high hematite continent reduces the permeability of source rocks (Ali *et al*. 2011). In addition, permeability is independent of the particle size of the hematite (Ali *et al*. 2011).

5 Conclusions

Quartz, kaolinite, montmorillonite, illite, calcite, and hematite are present in all marlstone and mudstone samples in the Mannar Basin. Clay mineralogy supports the characterization of paleoclimate such as warm/wet and arid climates. This study is helpful to get an idea about primary hydrocarbon migration in potential petroleum source rocks, based on parameters of porosity and permeability. Quartz, clay, carbonate, and hematite cementations reduce the primary migration of hydrocarbon in potential petroleum source rocks. However, feldspar dissolution enhances secondary porosity and permeability in potential petroleum source rocks.

Acknowledgments

The authors wish to greatly acknowledge the Petroleum Resources Development Secretariat (PRDS), Sri Lanka, for providing the cuttings samples. This study was financially supported by the University of Sri Jayewardenepura research grant (ASP/01/RE/SCI/2018/34). Two anonymous reviewers are acknowledged.

References

Ali A, Potter D, Imhmed S, Schleifer N. 2011. Quantifying the effects of core cleaning, core flooding and fines migration using sensitive magnetic techniques: implications for permeability determination and formation damage. *Petrophysics* 52(6): 444–451.

Bahlburg H, Floyd PA. 1999. Advanced techniques in provenance analysis of sedimentary rocks-Preface. *Sedimentary Geology* 124: 220

Bernet M, Bassett K. 2005. Provenance analysis by single-quartz-grain SEM-CL/optical microscopy. *Journal of Sedimentary Research* 75(3): 492–500. https://doi.org/10.2110/jsr.2005.038

Butt AS. 2012. Shale characterization using X-Ray diffraction. *Submitted in partial fulfillment of the requirements for the degree of Master of Engineering. Nova Scotia: Dalhousie University Halifax, August*.

Chester R, Elderfield H. 1968. The infrared determination of opal in siliceous deep-sea sediments. *Geochimica et Cosmochimica Acta* 32 (10): 1128-1140.

Chatterjee S, Goswami A, Scotese CR. 2013. The longest voyage: tectonic, magmatic, and paleoclimatic evolution of the Indian plate during its northward flight from Gondwana to Asia. *Gondwana Research* 23(1): 238–267. http://dx.doi.org/10.1016/j.gr.2012.07.001

Chen B, Wang F, Shi J Chen F, Shi H. 2019. Origin and sources of minerals and their impact on the hydrocarbon reservoir quality of the Paleogene Lulehe Formation in the Eboliang area, northern Qaidam Basin, China. *Minerals* 9(7): 436. https://doi.org/10.3390/min9070436

Chima P, Baiyegunhi C, Liu K, Gwavava O. 2018. Diagenesis and rock properties of sandstones from the Stormberg Group, Karoo Supergroup in the Eastern Cape Province of South Africa. *Open Geosciences* 10(1): 740–771. https://doi.org/10.1515/geo-2018-0059

Cooray PG. 1984. An introduction to the geology of Sri Lanka (Ceylon). *National Museums of Sri Lanka* 38.

Cornell RM, Schwertmann U. 2003. The iron oxides: structure, properties, reactions, occurrences and uses. Weinheim: Wiley-vch., 664.

Dera G, Pellenard P, Neige P, Deconinck JF, Pucéat E, Ommergues JL. 2009. Distribution of clay minerals in Early Jurassic Peritethyan seas: palaeoclimatic significance inferred from multiproxy comparisons. *Palaeogeography Palaeoclimatology Palaeoecology* 271(1-2): 39–51. https://doi.org/10.1016/j.palaeo.2008.09.010

Dowey PJ, Taylor KG. 2017. Extensive authigenic quartz overgrowths in the gas-bearing Haynesville-Bossier Shale, USA. *Sedimentary Geology* 356: 15–25. https://doi.org/10.1016/j.sedgeo.2017.05.001

Farmer VC. 1974. The infrared spectra of minerals:Mineralogical Society. London, Monograph 4: 539.

Ghosh SN. 1978. Infra-red spectra of some selected minerals, rocks and products. *Journal of Materials Science* 13(9): 1877-1886.

Hlavay J, Jonas K, Elek S, Inczedy J. 1978. Characterization of the particle size and the crystallinity of certain minerals by ir spectrophotometry and other instrumental methods II. Investigations on quartz and feldspar. *Clays and Clay Minerals* 26(2): 139–143. https://doi.org/10.1346/CCMN.1978.0260209

Hossain HMZ, Kawahata H, Sampei Y, Feakins SJ, Ratnayake AS. 2022. Organic matter and sedimentary accumulation rates in a transect of cores in the Bay of Bengal offshore Bangladesh and Andaman Sea offshore Myanmar. *Marine and Petroleum Geology* 142: 105769. https://doi.org/10.1016/j.marpetgeo.2022.105769

Jiang H, Pang X, Shi H, Yu Q, Cao Z, Yu R, Jiang F. 2015. Source rock characteristics and hydrocarbon expulsion potential of the Middle Eocene Wenchang formation in the Huizhou depression, Pearl River Mouth basin, south China sea. *Marine and Petroleum Geology* 67: 635–652. http://dx.doi.org/10.1016/j.marpetgeo.2015.06.010

Kampman N, Bickle M, Becker J, Assayag N, Chapman H. 2009. Feldspar dissolution kinetics and Gibbs free energy dependence in a CO_2-enriched groundwater system, Green River, Utah. *Earth and Planetary Science Letters* 284(3-4): 473–488. https://doi.org/10.1016/j.epsl.2009.05.013

Kularathna EKCW, Pitawala HMTGA, Senaratne A, Ratnayake AS. 2020. Play distribution and the hydrocarbon potential of the Mannar Basin, Sri Lanka. *Journal of Petroleum Exploration and Production Technology* 10(6): 2225–2243. https://doi.org/10.1007/s13202-020-00902-8

Kumar RS, Rajkumar P. 2014. Characterization of minerals in air dust particles in the state of Tamilnadu, India through FTIR, XRD and SEM analyses. *Infrared Physics & Technology* 67: 30–41. https://doi.org/10.1016/j.infrared.2014.06.002

Kumari N, Mohan C. 2021. Basics of clay minerals and their characteristic properties. *Clay Clay Miner* 24:1-29. https://doi.org/10.5772/intechopen.97672

Leontopoulou G, Christidis GE, Geraga M, Papatheodorou G, Koutsopoulou E. 2019. A novel mineralogical approach for provenance analysis of late Quaternary marine sediments: the case of Myrtoon Basin and Cretan Sea, Aegean, Greece. *Sedimentary Geology* 384: 70–84.

https://dx.doi.org/10.1016/j.sedgeo.2019.03.004 s

Liang C, Jiang Z, Zhang C, Guo L, Yang Y, Li J. 2014. The shale characteristics and shale gas exploration prospects of the Lower Silurian Long maxi shale, Sichuan Basin, South China. *Journal of Natural Gas Science and Engineering* 21: 636–648. https://doi.org/10.1016/j.jngse.2014.09.034

McBride EF. 1989. Quartz cement in sandstones: a review. *Earth-Science Reviews* 26(1-3): 69-112.

Milliken K. 2014. A compositional classification for grain assemblages in fine-grained sediments and sedimentary rocks. *Journal of Sedimentary Research* 84(12): 1185–1199. https://doi.org/10.2110/jsr.2014.92

Painter PC, Snyder RW, Starsinic M, Coleman MM, Kuehn DW, Davis A. 1981. Concerning the application of FT-IR to the study of coal: a critical assessment of band assignments and the application of spectral analysis programs. *Applied Spectroscopy* 35(5): 475–485.

Peng J, Milliken KL, Fu Q. 2020. Quartz types in the Upper Pennsylvanian organic-rich Cline Shale (Wolf camp D), Midland Basin, Texas: implications for silica diagenesis, porosity evolution and rock mechanical properties. *Sedimentology* 67(4): 2040–2064. https://doi.org/10.1111/sed.12694

Pollastro RM, Bohor BF. 1993. Origin and clay-mineral genesis of the Cretaceous/Tertiary boundary unit, the western interior of North America. *Clays and Clay Minerals* 41(1): 7–25. https://doi.org/10.1346/CCMN.1993.0410102

Pszonka J, Wendorff M. 2017. Carbonate cement and grains in submarine fan sandstones the Cergowa Beds (Oligocene, Carpathians of Poland) recorded by cathodoluminescence. *International Journal of Earth Sciences* 106(1): 269–282. https://doi.org/10.1007/s00531-016-1318-z

Raigemborn MS, Gómez-Peral LE, Krause JM, Matheos SD. 2014. Controls on clay minerals assemblages in an early Paleogene nonmarine succession: implications for the volcanic and paleoclimatic record of extra-Andean Patagonia, Argentina. *Journal of South American Earth Sciences* 52: 1–23. http://dx.doi.org/10.1016/j.jsames.2014.02.001

Rampe EB, Ming DW, Blake DF, Bristow TF, Chipera SJ, Grotzinger JP, Thompson LM. 2017. Mineralogy of an ancient lacustrine mudstone succession from the Murray formation, Gale crater, Mars. *Earth and Planetary Science Letters* 471:172–185. https://doi.org/10.1016/j.epsl.2017.04.021

Rao MV, Chidambaram L, Bharktya D, Janardhanan M. 2010. Integrated analysis of Late Albian to Middle Miocene sediments in Gulf of Mannar shallow waters of the Cauvery Basin, India: A sequence stratigraphic approach. *In Proceeding 8th Biennial International Conference and Exploration on Petroleum Geophysics Hyderabad* 1–9.

Ratnayake AS. 2021a. Late Cretaceous to Miocene paleoclimatic changes in the Indian Ocean: insights from the deepwater Mannar Basin, Sri Lanka. *Geo-Marine Letters* 41(3): 1-14. https://doi.org/10.1007/s00367-021-00710-x

Ratnayake AS. 2021b. Paleoenvironments and source rock potential of Dorado North well in the Mannar Basin (Indian Ocean). *Arabian Journal of Geosciences* 14(9): 1-9. https://doi.org/10.1007/s12517-021-07127-x

Ratnayake AS. 2022. An overview of organic geochemical indices to evaluate conventional petroleum source rocks: a summary of examples from the Indian Subcontinent. *Petroleum Science and Technology* 1-19. https://doi.org/10.1080/10916466.2022.2134893

Ratnayake AS, Kularathna CW, Sampei Y. 2018. Assessment of hydrocarbon generation potential and thermal maturity of the offshore Mannar Basin, Sri Lanka. *Journal of Petroleum Exploration and Production Technology* 8(3): 641–654. https://doi.org/10.1007/s13202-017-0408-1

Ratnayake AS, Sampei Y. 2015. Characterization of organic matter and depositional environment of the Jurassic small sedimentary basins exposed in the northwest onshore area of Sri Lanka. *Researches in Organic Geochemistry* 31(1): 15–28. https://doi.org/10.20612/rog.31.1_15

Ratnayake AS, Sampei Y. 2019. Organic geochemical evaluation of contamination tracers in deep-water well rock cuttings from the Mannar Basin, Sri Lanka. *Journal of Petroleum Exploration and Production Technology* 9(2): 989–996. https://doi.org/10.1007/s13202-018-0575-8

Ratnayake AS, Sampei Y, Kularathne CW. 2014. Stratigraphic responses to major depositional events from the Late Cretaceous to Miocene in the Mannar Basin, Sri Lanka. *Journal of Geological Society of Sri Lanka* 16(1): 5–18.

Ratnayake AS, Sampei Y, Kularathne CW. 2017. Current status of hydrocarbon exploration in Sri Lanka. *International Journal of Oil, Gas and Coal Technology* 16(4): 377–389. http://dx.doi.org/10.1504/IJOGCT.2017.10008362

Ruiz-Agudo E, King HE, Patiño-López LD, Putnis CV, Geisler T, Rodriguez-Navarro C, Putnis A. 2016. Control of silicate weathering by interface-coupled dissolution-precipitation processes at the mineral-solution interface. *Geology* 44(7): 567–570. https://doi.org/10.1130/G37856.1

Russell JD, Fraser AR. 1994. Infrared methods. In Clay Mineralogy: *Spectroscopic and chemical determinative methods* 11–67. https://doi.org/10.1007/978-94-011-0727-3_2

Sivakumar S, Ravisankar R, Raghu Y, Chandrasekaran A, Chandramohan J. 2012. FTIR spectroscopic studies on coastal sediment samples from Cuddalore District, Tamilnadu, India. *Indian Journal of Advances in Chemical Science* 1: 40–46.

Vaniman DT, Bish DL, Ming DW, Bristow TF, Morris RV, Blake DF, Spanovich N. 2014. Mineralogy of a mudstone at Yellowknife Bay, Gale Crater, Mars. *Science* 343(6169): 1243480. http://dx.doi.org/10.1126/science.1243480

White RJ, Spinelli GA, Mozley PS, Dunbar NW. 2011. Importance of volcanic glass alteration to sediment stabilization: offshore Japan. *Sedimentology* 58(5): 1138–1154. https://doi.org/10.1111/j.1365-3091.2010.01198.x

Worden RH, Morad S. 2000. Quartz cementation in oil field sandstones: a review of the key controversies. *Quartz Cementation in Sandstones* 29: 1–20. http://dx.doi.org/10.1002/9781444304237

Xu L, Shi Y, Xu C, Yang Y, Li H, Chai Z. 2013. Influences of feldspars on the storage and permeability conditions in tight oil reservoirs: a case study of Chang-6 group, Ordos Basin. *Petroleum Exploration and Development* 40(4): 481–487. http://dx.doi.org/10.1016/S1876-3804(13)60061-0

Yuan G, Cao Y, Schulz HM, Hao F, Gluyas J, Liu K, Li F. 2019. A review of feldspar alteration and its geological significance in sedimentary basins: from shallow aquifers to deep hydrocarbon reservoirs. *Earth-Science Reviews* 191: 114–140. https://doi.org/10.1016/j.earscirev.2019.02.004

Zachos JC, Shackleton NJ, Revenaugh JS, Palike H, Flower BP. 2001. Climate response to orbital forcing across the Oligocene-Miocene boundary. *Science* 292(5515): 274–278. http://doi.org/10.1126/science.105828

Zeng J, Yu C. 2006. Hydrocarbon migration along the Shengbei fault zone in the Bohai Bay Basin, China: the evidence from geochemistry and fluid inclusions. *Journal of Geochemical Exploration* 89(1-3): 455–459. https://doi.org/10.1016/j.gexplo.2005.11.031

Zou C, Dong D, Wang S, Li J, Li X, Wang Y, Cheng K. 2010. Geological characteristics and resource potential of shale gas in China. *Petroleum Exploration and Development* 37(6): 641–653. http://dx.doi.org/10.1016/S1876-3804(11)60001-3